A Capacitive Microcantilever: Modelling, Validation, and Estimation Using Current Measurements

Mariateresa Napoli
e-mail:napoli@engineering.ucsb.edu

Bassam Bamieh
e-mail:bamieh@engineering.ucsb.edu

Kimberly Turner
e-mail: turner@engineering.ucsb.edu

Department of Mechanical Engineering,
University of California,
Santa Barbara, CA 93106

We present a mathematical model for the dynamics of an electrostatically actuated microcantilever. For the common case of cantilevers excited by a periodic voltage, we show that the underlying linearized dynamics are those of a periodic system described by a Mathieu equation. We present experimental results that confirm the validity of the model, and in particular, illustrate that parametric resonance phenomena occur in capacitively actuated micro-cantilevers. We propose a system where the current measured is used as the sensing signal of the cantilever state and position through a dynamical observer. By investigating how the best achievable performance of an optimal observer depends on the excitation frequency, we show that the best such frequency is not necessarily the resonant frequency of the cantilever. [DOI: 10.1115/1.1767851]

1 Introduction

The recent advances in the field of miniaturization and micro fabrication have paved the way for a new range of applications, bringing along the promise of unprecedented levels of performance. In particular, scanning probe devices have proven to be extremely versatile instruments, with applications that range from surface imaging at the atomic scale [1], to ultra high density data storage and retrieval [2], and to biosensors [3,4], to cite but a few.

The working principle for most of these devices is based on a measurement of displacement. As an example, consider imaging in atomic force microscopy: the topography of a sample is reconstructed from the displacement of the cantilever-probe, caused by the interaction forces with the sample [5,6]. In biosensors applications the displacement of a cantilever can be related to the binding of molecules on the (activated) surface of the cantilever beam, and is therefore used to compute the strength of these bonds, as well as the presence of specific reagents in the solution under consideration [7,8]. It is clear that the sensitivity of these devices strongly depends on the smallest detectable motion, which poses a constraint on the practically vs. theoretically achievable performance. In order to make the gap between the two smaller, while at the same time providing compactness of devices and faster dynamics, much of the research effort has been focused on the design of integrated detection schemes.

The most common solutions for integrated detection make use of the piezoresistive, [9,10], piezoelectric [11–13], thermal expansion [14] or capacitive effects [15–17]. A major advantage of capacitive detection, is the fact that it offers both electrostatic actuation as well as integrated detection, without the need for an additional position sensing device. The common scheme used in capacitive detection is to apply a second AC voltage at a frequency much higher than the mechanical bandwidth of the cantilever. The current output at that frequency is then used to estimate the capacitance, and consequently the cantilever position. This sensing scheme is the simplest position detection scheme available, however, it is widely believed to be less accurate than optical levers or piezoresistive sensing.

The device that we propose is an electrostatically actuated microcantilever. More precisely, in our design the microcantilever constitutes the movable plate of a capacitor and its displacement is controlled by the voltage applied across the plates. In order to measure the cantilever displacement, we propose a novel scheme that avoids the use of a high frequency probing signal by the use of a dynamical state observer, whose input is the current through the capacitive cantilever. For the purpose of implementation, this scheme offers significant advantages as it involves simpler circuitry. By using an optimal observer, or by tuning the observers gains, it is conceivable that a high fidelity position measurement can be obtained, thus improving resolution in atomic force microscopy applications.

In this paper, we present a model for this electrostatically actuated microcantilever. Using simple parallel plate theory and for the common case of sinusoidal excitation, it turns out that its dynamics are governed by a special second order linear periodic differential equation, called the Mathieu equation. We produce experimental evidence that validates the mathematical model, including a mapping of the first instability region of the Mathieu equation.

The optimal observer problem that was formulated also in [18] is solved here following a different and simpler approach. This optimal design is then used as an analysis tool to select the frequency of excitation that corresponds to the best achievable observer performance. In other words, the optimal observer design is used to actually design the system (rather than the observer), by selecting the excitation frequency that produces the least estimation error. Interestingly, it turns out that this frequency is not necessarily the resonant frequency of the cantilever, and it depends on the statistics of the measurement and process noise.

After the optimal excitation frequency is selected, we design a suboptimal reduced order observer, whose parameters are tuned to match the optimal performance index as close as possible. The extension of these results to the array configuration is the subject of our current research.

The paper is organized as follows: In Section 2, we develop the mathematical model of an electrostatically actuated cantilever. In Section 3, we present the experimental results that validate the model including, in particular, the mapping of the first instability region of the Mathieu equation. In Section 4, we pose the optimal observer problem for time varying systems and in Section 5, we design a suboptimal reduced order observer. Finally, we present our conclusions in Section 6.

Contributed by the Dynamic Systems, Measurement, and Control Division of THE AMERICAN SOCIETY OF MECHANICAL ENGINEERS for publication in the ASME JOURNAL OF DYNAMIC SYSTEMS, MEASUREMENT, AND CONTROL. Manuscript received by the ASME Dynamic Systems and Control Division July 2, 2003 final revision, November 3, 2003 Associate Editor: R. Gao.

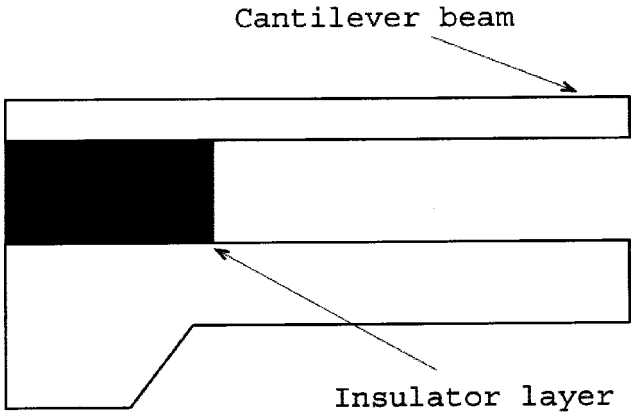

Fig. 1 A schematic of an electrostatically driven cantilever

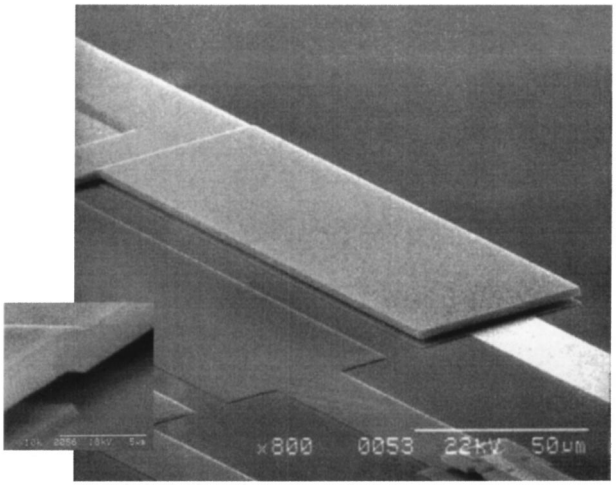

Fig. 2 SEM image of a polySi cantilever. The inset shows details of the mechanical connection to the base.

2 Model Description for a Single Cantilever

The schematic of a single cantilever sensor is shown in Fig. 1. It consists of two adjacent electrically conductive beams forming the two plates of a capacitor. One of the beams is rigid, while the other (hereafter referred to as the cantilever) is fairly soft and represents the movable part of the structure.

If the length of the cantilever is much bigger than its distance from the bottom plate, the capacitance is given by

$$C(z)=\frac{\epsilon_o A}{d-z}, \tag{1}$$

where $\epsilon_o=8.85\,10^{-12}$ As/Vm is the permittivity in vacuum, A is the area of the plates, d is the gap between them and z is the vertical displacement of the cantilever from its rest position.

The attractive force, F_a, between the capacitor plates generated by applying a voltage $V(t)$, can be easily found to be

$$F_a=\frac{1}{2}\frac{\epsilon_o A}{d^2}\frac{V^2(t)}{\left(1-\frac{z}{d}\right)^2}\approx\frac{1}{2}\frac{\epsilon_o A}{d^2}\left(1+2\frac{z}{d}\right)V^2(t),$$

where the approximation holds when $z/d\ll 1$.

Only few algebraic steps are sufficient to derive the equation of motion of the cantilever, which is treated as a lumped-parameter system, and hence described by taking into account its first bending mode only, and neglecting all higher order flexible modes. This approximation is quite common in the study of the dynamics of scanning probe cantilevers [5,19,20]. It follows that, if the voltage applied is $V(t)=V_o\cos\omega_o t$, the equation of motion is given by

$$z''+cz'+(a-2q\cos 2t)z=u_f(t), \tag{2}$$

where the prime denotes the derivative with respect to the scaled time $\tau=\omega_o t$; c is a small damping coefficient, both from air friction and structural losses, $a=k/m\omega_o^2-1/2\epsilon_o AV_o^2/md^3\omega_o^2$, k is the spring constant of the cantilever, $q=\epsilon_o AV_o^2/4md^3\omega_o^2$, and $u_f(t)=qd\cos^2(t)$.

Equation (2) is an instance of the well-known Mathieu equation. Its properties are briefly discussed in Section 3. Here we just point out that when $u_f(t)\equiv 0$ and $c=0$ this equation has very peculiar stability properties, that have been extensively investigated. As a and q vary in **R**, its stable solutions can be periodic, but they never decay to zero. In the case of our interest, where $u_f(t)\neq 0$ and periodic, we can prove that, for any pair of parameters a and q, the forced equation retains the same stability properties as the unforced one.

We consider the current generated as the output y of the system. Its first order approximation is given by

$$y=c_1(t)z+c_2(t)z'+v_f(t), \tag{3}$$

where $c_1(t)=-\epsilon_o AV_o w_o/d^2\sin t$, $c_2(t)=\epsilon_o AV_o/d^2\cos t$, and $v_f(t)=\epsilon_o AV_o w_o/d\sin t$.

Introducing the vector $x=[z\ \dot{z}]^T$, we can derive from (2) and (3) the state space representation of the cantilever model

$$\begin{aligned} x'&=A(t)x+B(t)u_f(t)\\ y&=C(t)x+v_f(t), \end{aligned} \tag{4}$$

where

$$A(t)=\begin{bmatrix} 0 & 1\\ -a+2q\cos 2t & -c\end{bmatrix};$$

$$B=\begin{bmatrix}0\\1\end{bmatrix}$$

and

$$C(t)=[c_1(t)\ c_2(t)].$$

Note that (4) is a linear, time-varying and T-periodic model, with $T=2\pi$. The next section is devoted to presenting the results of the experiments that we performed to validate the model.

3 Experimental Validation of the Cantilever Model

The device we have used in our experimental setup was a 200 μm×50 μm×2 μm highly doped polysilicon cantilever, fabricated using the MUMPS/CRONOS process, and with a gap between the electrodes of about 2 μm. Figure 2 is a micrograph of the actual device. The mechanical response of the cantilever was tested in vacuum ($p=8mT$), using laser vibrometry [21] to measure its displacement and velocity near the free end, when electrostatically driven with different AC voltage signals.

The first experiments we performed aimed at identifying the system as a simple mass-spring-damper model. As a matter of fact, when the amplitude V_o of the AC actuation voltage is small enough, the coefficient q in equation (2) is negligible, and the beam can be described approximately by an ordinary second order differential equation

$$\ddot{z}+2\xi\omega_r\dot{z}+\left(\omega_r^2-\frac{1}{2}\omega_e^2V_o^2\right)z=u(t).$$

Figure 3 shows the magnitude, both measured and identified, of the frequency response of this model, excited by a square-rooted sinusoidal signal. A least square fitting of the data gives a resonant

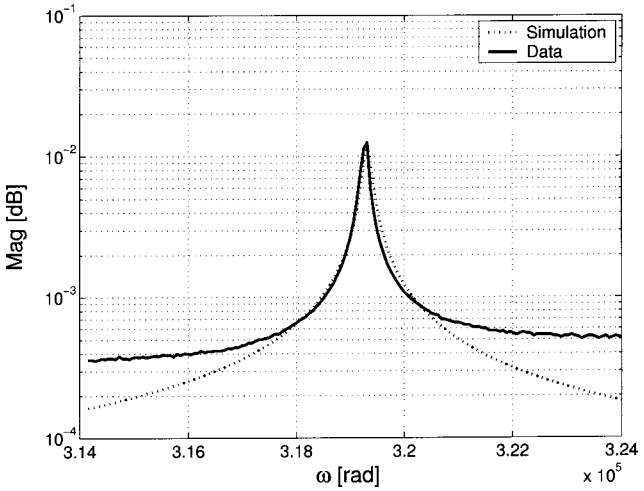

Fig. 3 Frequency response of the capacitive cantilever: the dashed line corresponds to measured data, the solid one is its least square fit

frequency of approximately $f_r = 50{,}800$ Hz, a damping coefficient $\xi = 2.1 \times 10^{-4}$, while the quality factor $Q = 2200$ turns out, as expected, to be quite high. The values of these parameters were confirmed by time domain identification experiments as well. If we consider that the Young's modulus for Cronos' polysilicon is $E = 158 \pm 10$ GPa, its density is $\rho = 2300$ Kg/m^3, we can infer from the identified data that the effective length of the capacitor plate is about $L = 160$ μm.

A second set of experiments aimed at identifying the value of the so-called "electrostatic resonance," ω_e, responsible for the shift in the effective resonant frequency, ω_{eff}, of the cantilever with the voltage applied, $\omega_{\text{eff}}^2 = \omega_r^2 - 1/2\omega_e^2 V_o^2$. A linear fit of the experimental data points gives a value of $\omega_e^2 = 2.63e^8$ [rad/V^2], in good agreement with its theoretical value (see Fig. 4).

As the amplitude of the driving signal increases, so does the value of q and this approximation of the model is no longer appropriate. Therefore, we have to return to the original Eq. (2), which will be analyzed in detail in the next section.

3.1 The Mathieu Equation and Parametric Resonance. When the amplitude of the forcing signal is large, the time invariant approximation introduced in the previous section is not sufficient to describe the rich dynamics exhibited by the system and we need to refer again to Eq. (2). This equation is an example of a damped Mathieu equation with forcing, a well known and studied periodic differential equation. As a matter of fact, an extensive literature exists on its standard form

$$z'' + (a - 2q\cos 2t)z = 0, \tag{5}$$

that has neither damping nor external forcing and that was first introduced by Mathieu to model the vibrational modes of a stretched membrane having an elliptical boundary.

The stability of linear periodic differential equations, like Eq. (2), is determined by the eigenvalues of its state transition matrix over one period. More precisely, the equation is stable if these eigenvalues are smaller than one, and unstable if at least one is larger than one [22]. Unfortunately, it is usually not possible to compute this matrix analytically, hence the analysis makes use of approximate tools, like averaging or perturbation-methods. For the specific case of Eq. (5), a detailed derivation, using perturbation methods, of the stable/unstable regions as a function of the parameters a and q can be found for instance in [23]. Figure 5 portrays these characteristic tongue-like shaped regions. In particular, and we omit here the details for the sake of brevity, it is not difficult to prove that instabilities occur at $a = n^2$, $n \in \mathbb{N}$.

In terms of the physical parameters of the device, the driving frequencies that cause unstable responses in the system are given by

$$\omega_o \approx \frac{2\omega_r}{n} \quad n \in \mathbb{N},$$

when using a square-rooted sinusoidal driving signal. Similarly, the boundaries of the first instability region, given by $a = 1 \pm q$ for (5), in terms of frequency and amplitude of excitation turn out to be defined by

$$\omega_o^2 = 4\omega_r^2 - 4\left(1 \mp \frac{1}{2}\right)\frac{\epsilon A V_o}{md^3}.$$

It is worth noting at this point that the presence of a damping term, whose existence we have neglected so far, has the effect of shifting the tongues upwards in the a-q parameter space. In our setup, this is of little consequence, because the magnitude of the shift is quite small. However this is not always the case and in fact it is the reason why parametric resonance is difficult to observe at the macroscale. Figure 6 is a comparison between the experimental data relative to the boundaries of the first instability region, and the same curves obtained from two sets of parameters: the solid lines come from fitting these experimental data points, the dash-

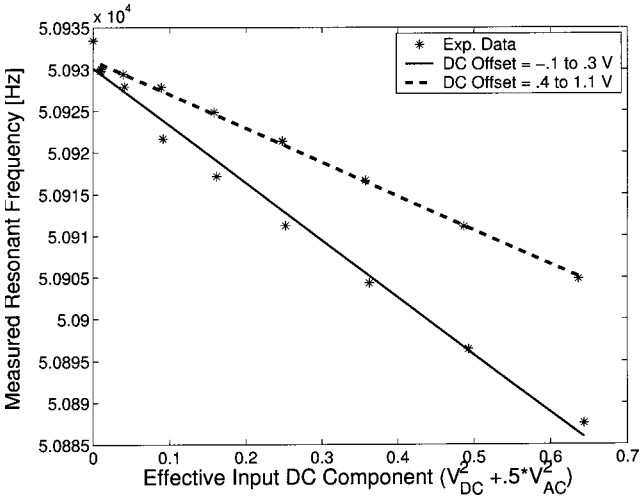

Fig. 4 Electrostatic resonance. The dots represent measured values of resonance frequency, the solid line is their linear fit.

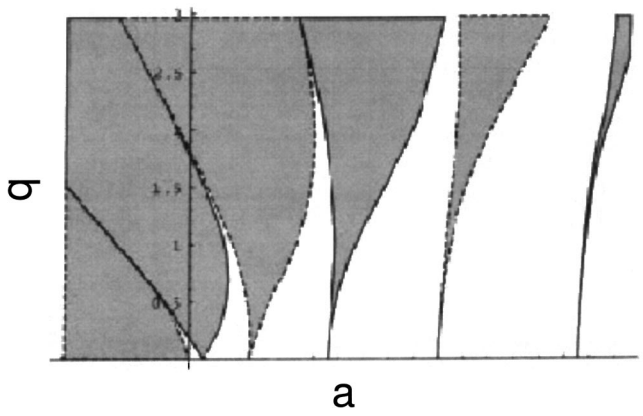

Fig. 5 Mathieu equation: the shaded areas correspond to unstable behavior

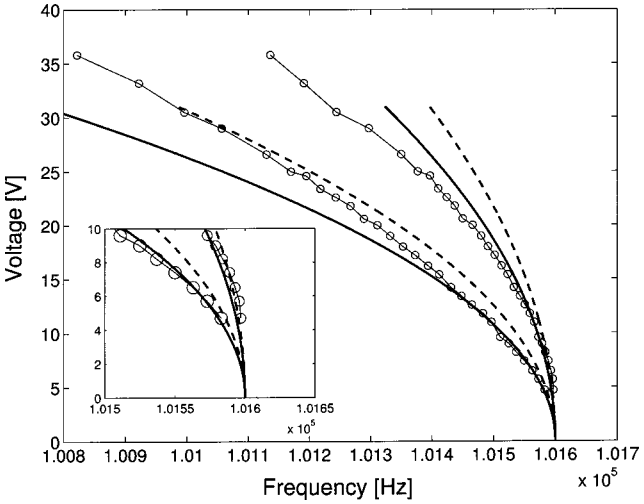

Fig. 6 First instability region: experimental data points (circles) and curves with identified parameters. Inset: effect of damping visible on experimentally measured data, marked with circles.

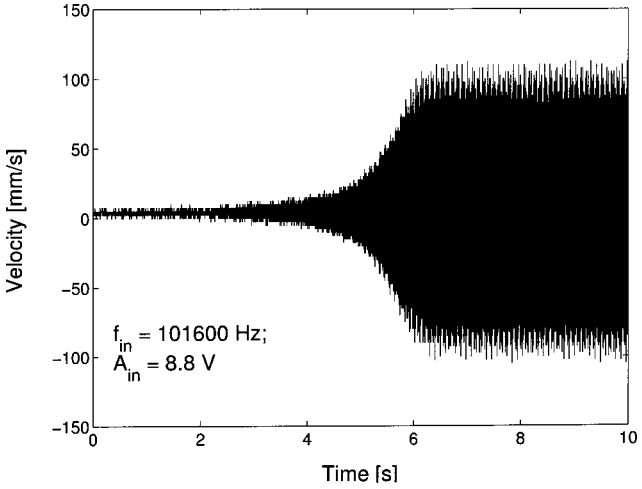

Fig. 8 Exponential growth of oscillation following parametric excitation

dotted ones come from the frequency response identification. The inset shows the experimentally observed upwards shift of the unstable region with damping.

Inside the instability region the cantilever oscillation does not grow unbounded, as predicted from the previous linear analysis. In reality, physical limiting nonlinear effects always come into play and cause the system to settle down into a steady state response [24]. As a consequence, the linear spring model needs to be corrected to include a cubic term

$$z'' + cz' + (a - 2q\cos 2t)z + \mathbf{a_2 z^3} = u_f(t), \tag{6}$$

whose origin is both mechanical, because of the large displacement of the beam, and electrostatic.

What we really see when driving the cantilever in parametric resonance regime is a subharmonic 2:1 oscillation of the beam [24], which vibrates at half the frequency of excitation, as shown in Fig. 7, which reproduces data collected from the oscilloscope. Note also that during the transition from non-parametric to parametric region, the response shows a characteristic exponential growth (see Fig. 8). Above the critical driving voltage amplitude, and for driving frequencies near the first parametric resonance, the frequency response of the cantilever has the shape depicted in Fig. 9. The two curves reproduced represent the data collected by sweeping the driving frequency from low to high (+ points) and from high to low (*o* points), as indicated by the arrows. The vertical axis represents the amplitude of the periodic (half frequency) velocity of the beam, while the horizontal axis is the frequency of excitation.

This kind of plot is typical of oscillators having a cubic nonlinearity (Duffing). What is worth pointing out here is the sharp transition of the output response (vertical segment of + data) that marks the entrance into the parametric region. Since this transition always occurs for the same value ω_1, related to the resonant frequency of the beam, the phenomenon has potentially many applications, from the realization of mechanical filters to extremely sensitive mass sensors. Inside the parametric region, the system exhibits a stable periodic oscillation, whose amplitude decreases as the driving frequency increases, until it goes to zero upon exiting the region. Note that the size of the interval $[\omega_1\ \omega_2]$ corresponds to the width of the parametric tongue represented in Fig. 6 for the input amplitude value considered. If we invert the process and start decreasing the frequency, the output amplitude,

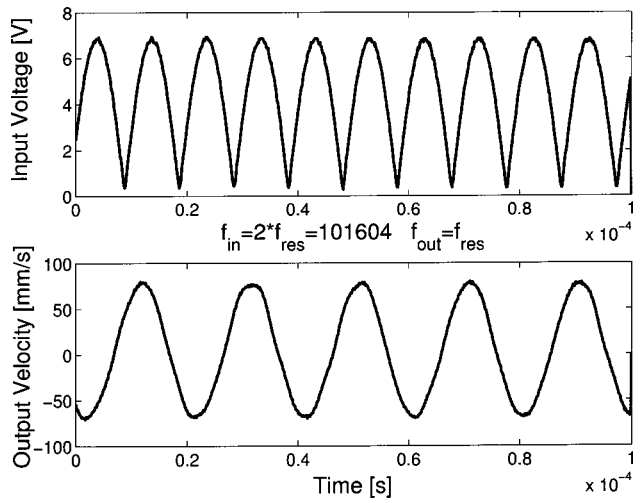

Fig. 7 Cantilever response in parametric resonance (oscilloscope data)

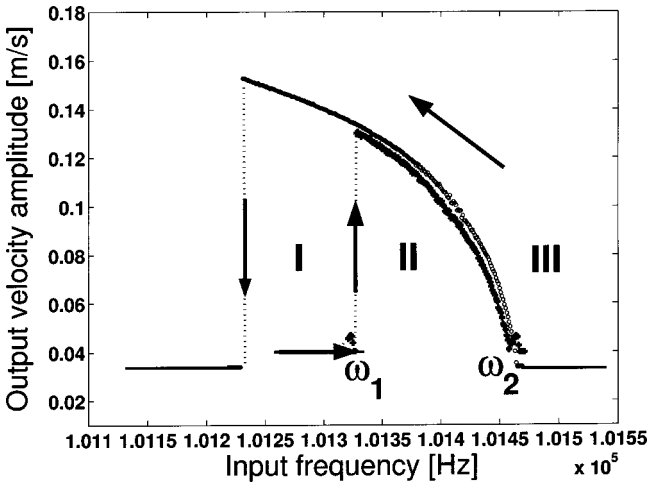

Fig. 9 Frequency response above critical driving voltage amplitude ($A = 10$ V). The solid and dashed lines have been added to the experimental data points (marked with *o* and +) to facilitate the reading.

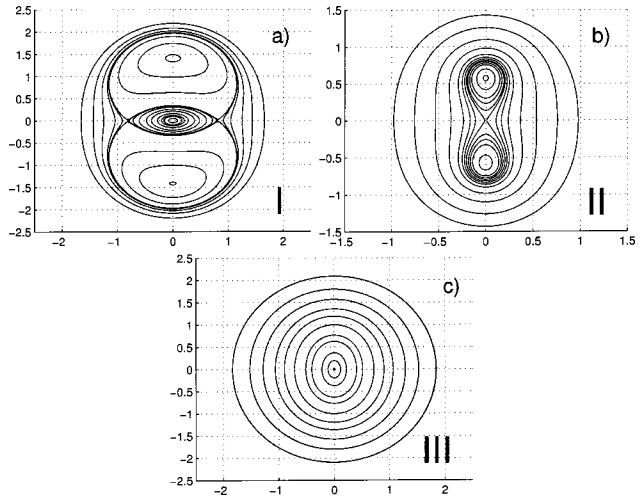

Fig. 10 Phase portrait of Eq. (6). The labelling corresponds to the regions of Fig. 9.

which is zero at the beginning, starts to increase as soon as we enter the parametric region. This subharmonic periodic solution remains stable even after leaving the region and its amplitude keeps increasing. However, it is only a matter of time before it collapses to zero. The location of this second jump is not predictable and depends on the amplitude of the frequency decrements.

This behavior can be explained and predicted mathematically by using averaging [24,25]. As a matter of fact, the relative magnitude of the coefficients in Eq. (6) allows us to rewrite it in the following fashion

$$\ddot{z}+c\dot{z}+z=\epsilon(-(a_1+2q_1\cos 2t)z-a_{31}z^3), \tag{7}$$

where $a=1+\epsilon a_1$, $q_1=q/\epsilon$ and $a_{31}=a_3/\epsilon$. We refer the interested reader to [24–26] for a detailed analysis. In brief, we assume the solutions to be of the form $z(t)=A(t)\cos t+B(t)\sin t$, with A and B slowly varying functions of time. It can be shown [24] that these coefficients are described by the following system of nonlinear coupled ordinary differential equations (ODEs)

$$\begin{aligned} A' &= \frac{1}{2}(a_1-1)B+\frac{3a_{31}}{8}B(A^2+B^2), \\ B' &= -\frac{1}{2}(a_1+1)A-\frac{3a_{31}}{8}A(A^2+B^2), \end{aligned} \tag{8}$$

which can be solved numerically to obtain the regions of parametric resonance. The phase portrait resulting from this analysis is shown in Fig. 10. Corresponding regions in the parameter space of Figs. 9 and 10 have been labeled with the same number, to highlight the fact that the theoretical analysis indeed confirms the experimental findings.

4 The Optimal Observer Problem

In this section, we address the problem of designing a dynamical system capable of providing an estimate $\hat{z}$ for the cantilever displacement, based on the measurement of the current generated. This approach to sensing is particularly advantageous from the point of view of implementation, as it requires a simpler circuitry. As a matter of fact, the extraction of the desired information is left to a software elaboration of the measurements.

In the LFT framework, the observer problem can be formulated as an $\mathcal{H}_\infty$ filtering problem [18], by defining the variable $\tilde{z}=z-\hat{z}$ (estimation error), and considering the generalized plant (see Fig. 11)

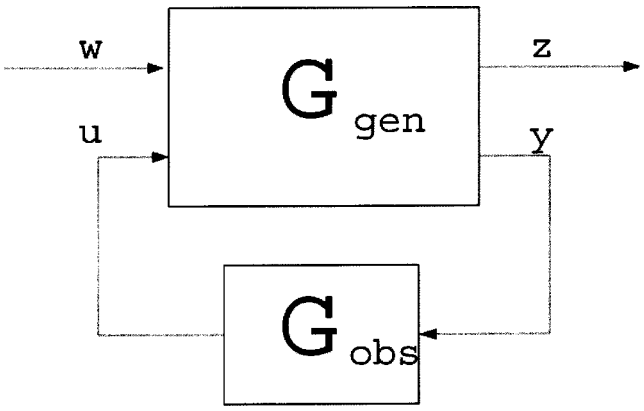

Fig. 11 A schematic of the observer problem

$$G_{gen}:=\begin{bmatrix} \mathrm{A(t)} & [\mathrm{M}\ \ 0] & 0 \\ \mathrm{I} & 0 & -\mathrm{I} \\ \mathrm{C(t)} & [0\ \ \mathrm{N}] & 0 \end{bmatrix}=\begin{bmatrix} \mathrm{A(t)} & B_1 & 0 \\ C_1 & 0 & D_{12} \\ C_2(t) & D_{21} & 0 \end{bmatrix}, \tag{9}$$

where the exogenous input $w=[d\ n]^T$ represents process and measurement noise, the matrices $A(t)$, $C(t)$ are as in (4) and the input $u=\hat{z}$ is the output of the observer system. Notice that we don't need to account for the signals u_f and v_f in (4): since they are known, their presence does not affect the observer design. In this framework, the optimal observer problem amounts to finding a dynamical system G_{obs} such that the $\mathcal{H}_\infty$ norm of the transfer function $T_{\tilde{z}w}$ from w to $\tilde{z}$ is minimized. If the system is time-invariant, and has the structure of (9), it can be proved that G_{obs} is an observer, whose gain L comes from the solution of an appropriate algebraic Riccati equation.

It turns out [27] that the same holds true in the time varying case, where the algebraic equation is replaced by a periodic differential Riccati equation

$$\begin{aligned} \dot{P}(t)=A(t)P(t)+P(t)A(t)'-P(t)C(t)'R^{-1}C(t)-\frac{1}{\gamma^2}IP(t) \\ +B(t)B(t)'. \end{aligned} \tag{10}$$

As a matter of fact, if the periodic non-negative definite solution of this equation, $P(t)$, is stabilizing, the optimal filter is an observer given by

$$\dot{\hat{z}}=A(t)\hat{z}+\mathbf{P(t)C(t)}'[y(t)-C(t)\hat{z}].$$

While we do not want necessarily to implement this optimal observer, we want to propose a method where we use the driving frequency ω_o as a design parameter in (10) and tune its value so that the closed loop system has the minimum attainable H_∞ norm.

This procedure requires to compute the periodic stabilizing solution of (10) for different values of the driving frequency ω_o. In order to do so, we defined the mapping $\mathcal{P}:R^{n\times n}\rightarrow R^{n\times n}$,

$$\mathcal{P}(M)=M-P(T),$$

where $P(T)$ is the solution, computed at time T of

$$\dot{P}=AP+PA'-PRP+Q,\quad P(0)=M.$$

If M is a matrix corresponding to any of the steady state periodic solutions, then $\mathcal{P}(M)=0$. Thus the problem is converted to finding the fixed points of this equation. This can be done numerically by using the secant method and defining the iterative scheme:

$$M_{k+1}=M_k-[M_k-M_{k-1}][\mathcal{P}(M_k)-\mathcal{P}(M_{k-1})]^{-1}\mathcal{P}(M_k).$$

Figure 12 describes the dependence of this norm on the frequency of excitation ω_o. The parameters of the cantilever used in

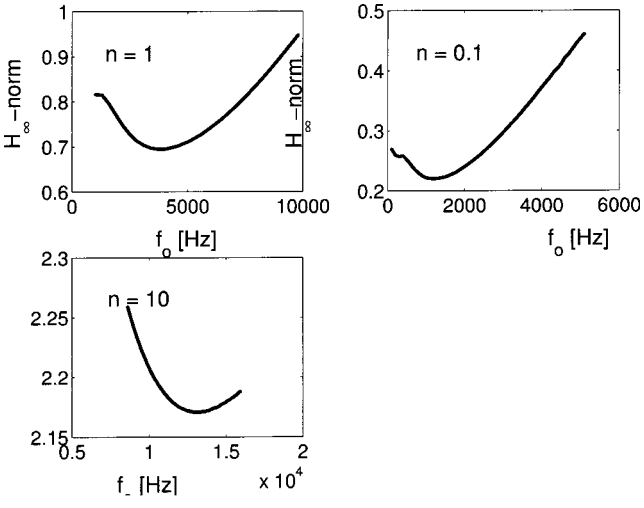

Fig. 12 H_∞-norm vs. frequency of excitation

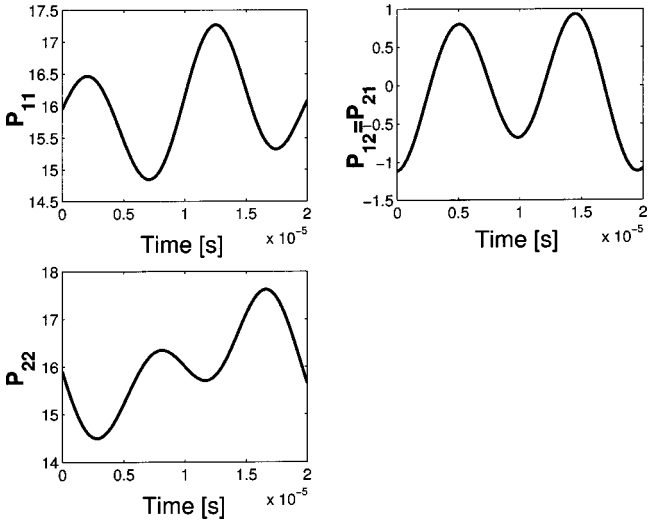

Fig. 14 Components of $P(t)$

this analysis are those indicated in the previous Section. In particular, we used the effective value of the length obtained by identification. Notice that the minimum is reached at different values of the driving frequency, depending on the measurement noise weight n and not necessarily coinciding with the resonance frequency. We note here that the analysis in this paper is done solely for the optimal observer design problem. In any realistic application of micro-cantilevers, there will be other control objectives as well. The problem set up then would involve a compound cost function that involves both observations and control. For such a problem, the best driving frequency will probably be different than the ones obtained here, and its value will depend on the particular tradeoffs between control and estimation. The framework we present in this paper should be easily extended to incorporate control objectives as well.

5 The Reduced Order Observer

A reduced order observer allows us to exploit the information about the state of the system that is provided by the output signal and leave to the observer the task of estimating a smaller portion of the state vector. We refer the interested reader to any book on linear systems theory for the details of this standard technique. Here we just want to provide the expression of the matrix T^{-1} that defines the required change of coordinates,

$$T^{-1}=\begin{bmatrix}H(t)\\ C(t)\end{bmatrix}=\begin{bmatrix}c_2^{-1}\cos t & -c_1^{-1}\sin t\\ c_1\sin t & c_2\cos t\end{bmatrix},$$

where c_i, $i=1, 2$ are the constant coefficients of $c_i(t)$ in (4), $T^{-1}\in\mathbf{C}^1$ and $\det(T^{-1})=1$ at each t. Notice that to be well-defined, this change of coordinates requires to consider a 'noiseless' output, i.e. $\tilde{y}=C(t)x$.

The equations of the observer turn out to be

$$\dot{\hat{v}}=(A_{11}(t)+L(t)A_{21}(t))\hat{v}+M(t)y$$

$$\hat{z}=T(t)\begin{bmatrix}\hat{v}-L(t)y\\ y\end{bmatrix},$$

where A_{11}, A_{21}, M are π-periodic matrices that can be computed from the system matrices in (4). $L(t)$ is the design parameter, through which we can adjust the behavior of the observer.

The state estimation error, $e_z=z-\hat{z}$ is described by

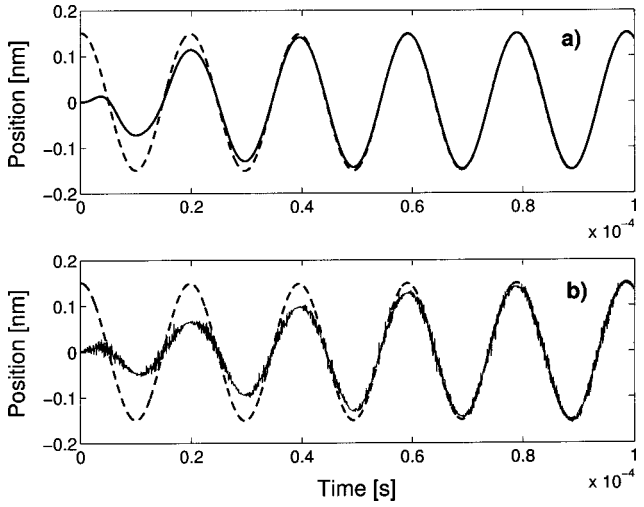

Fig. 13 Performance of the observers in the presence of measurement noise and initial estimation error. The dashed line is the measured position signal, the solid line its estimate. a) Optimal observer b) Reduced order observer.

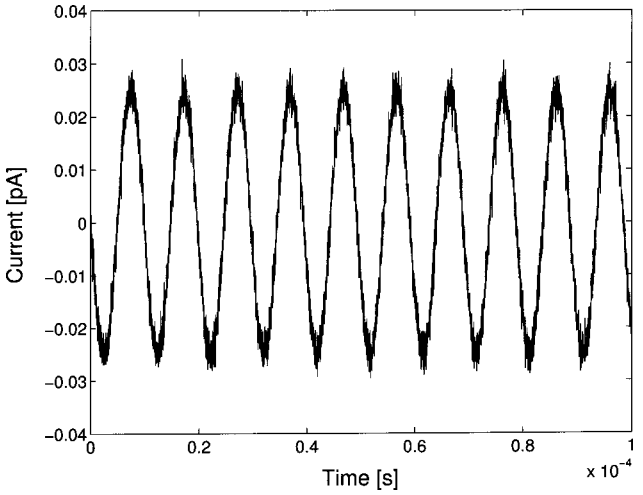

Fig. 15 Expected current signal from experimental velocity and position data

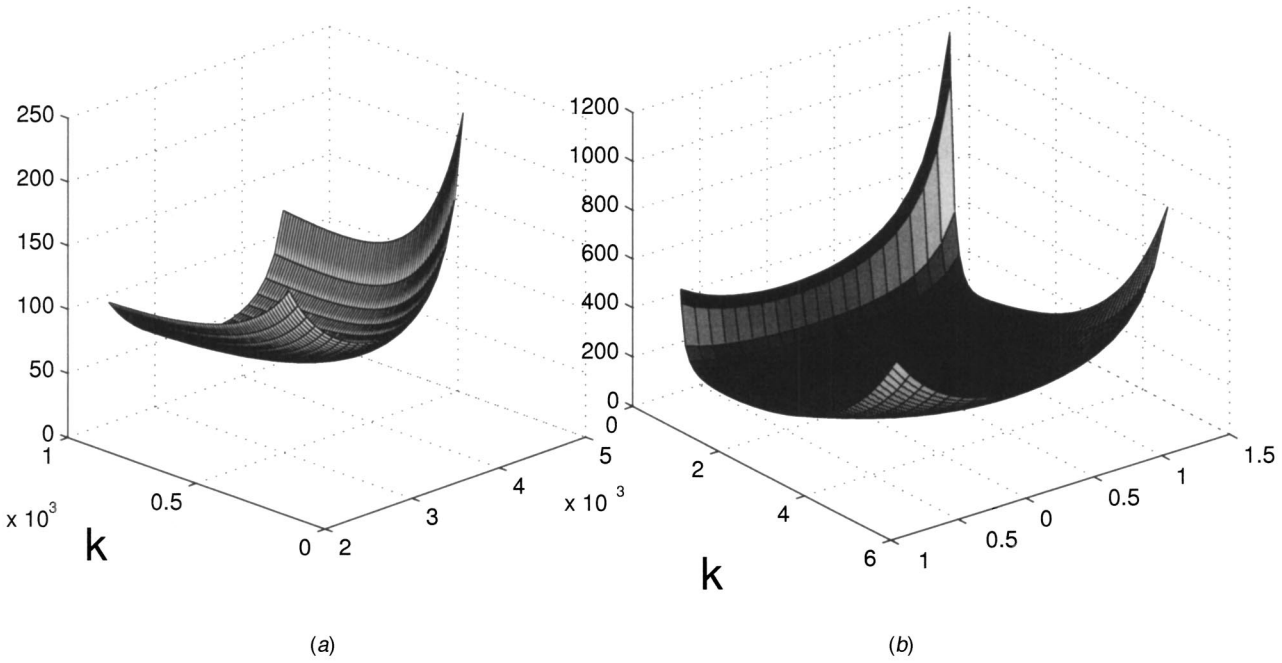

Fig. 16 Estimation error for different values of the observer gain: a) $k>0$ $\cos(\phi)<0$, b) $k<0$ $\cos(\phi)>0$

$$e_z = T\begin{bmatrix} e_v \\ 0 \end{bmatrix} + \begin{bmatrix} 0 & 0 \\ & D_z(t) \\ 0 & 0 \end{bmatrix} w, \tag{11}$$

where e_v is governed by the equation $\dot{e}_v = (A_{11} + LA_{21})e_v + B_v(t)w$ and the matrices D_z, B_v are known functions of the system matrices.

$L(t)$ needs to be chosen so that (11) is asymptotically stable. For a T-periodic system this is equivalent to say that its characteristic multipliers, which are the eigenvalues of the state transition matrix $\mathbf{\Phi}$ over on period T, are in norm less than 1, $|\lambda(\mathbf{\Phi}(T))|<1$. Since we are dealing with a scalar system, $\mathbf{\Phi}(T)$ can be easily computed

$$\mathbf{\Phi}(T) = e^{\int_0^T (A_{11}+LA_{21})(\sigma)d\sigma},$$

and the condition on the characteristic multipliers is equivalent to the condition $\int_0^T (A_{11}+LA_{21})(\sigma)d\sigma<0$. While it can be seen that a static gain L would be enough to guarantee the stability of the error dynamics (see Fig. 13), if we choose it time-varying, $L(t)=k\cos(\alpha t+\phi)$, we can use the parameters α, k and ϕ to optimize its performance. In particular, it can be seen that for a sinusoidal input the stability condition is met for $\alpha=2$ and by taking $c/2+kd_4\pi\cos\phi>0$, where c is the damping coefficient of (2) and d_4 is a known function of the system parameters.

Figure 13 compares the performance of a static reduced order observer ($L=L_0$) to the optimal observer described in the previous section ($L=P(t)C(t)'$). Figure 14 shows the components of $P(t)$, obtained as a solution to (10) for $\gamma=10$. At this moment the implementation of the circuit to measure the current is still under study. Therefore, we have generated the current signal starting from the experimentally measured velocity and position, using the non linear model $i(t)=d/dt[C(x,t)V(t)]$, where $C(x,t)$ is the capacitance (1), and $V(t)$ is the input voltage. Gaussian noise, corresponding to a S/N of approximately 12.5, has been added to mimic a real measurement (see Fig. 15).

As can be seen, the estimate of both observers converges quite fast to the measured displacement signal: only four cycles for the optimal observer and six for the reduced order observer. However, the latter is affected more heavily by the presence of noise, as expected. The price to pay for its simpler dynamics is a degradation of its performance.

For this reason, we want to select the parameters of this observer not only to ensure stable error dynamics, but also to optimize its performance, with the $\mathcal{H}_\infty$-norm as its measure. The computation of the $\mathcal{H}_\infty$-norm of a periodic system, as our closed loop system is, represents a difficulty. We have overcome it by using lifting [28] and fast-sampling [29] techniques. In fact it has been proven in [29] that as the fast sampling rate $f=N/T$, T period of the system, grows, the approximate sampled model converges to the original one with a rate of $1/N$.

Figure 16 depicts the value of the closed loop norm as k and ϕ vary in $\mathbf{R}$ and $[0\ 2\pi)$ respectively. Based on this plot, a better informed choice of k and ϕ turns out to be $k=0.001$ and $\phi=3.63$, which give $\mathcal{H}_\infty$-norm$=45$.

6 Conclusions

A mathematical model for an electrostatically actuated microcantilever has been derived based on the idealization of a movable plate capacitor. In contrast to standard capacitive sensing schemes which use a high frequency parasitic signal, we proposed an observer based design using the current generated in the microcantilever plates. Our model for the cantilever dynamics is governed by a special second order differential equation with periodic coefficients, the Mathieu equation. We have provided experimental validation of the mathematical model, which included the mapping of the first region of instability of the Mathieu equation. We have formulated the optimal observer problem for the cantilever based on current measurement. The performance of this sensing scheme in simulations proves to be excellent.

Further work on these devices involves on the one hand the experimental implementation of the current sensing scheme, which involves the measurement of fairly small currents in the range of pico-Ampers. On the other hand, the extension of this work to coupled multi-micro-cantilveres is also being pursued.

Acknowledgments

The first author would like to thank Wenhua Zhang and Rajashree Baskaran for the precious help offered during the testing of the device.

This work partially supported by a National Science Foundations grant ECS-0323814.

References

[1] Indermhule, P. et al., 1997, ''Fabrication and Characterization of Cantilevers With Integrated Sharp Tips and Piezoelectric Elements for Actuation and Detection for Parallel AFM Applications,'' Sens. Actuators, A, **A60**(1–3), pp. 186–190.
[2] Despont, M. et al., 2000, ''VLSI-NEMS Chip for Parallel AFM Data Storage,'' Sens. Actuators, A, **A80**(2), pp. 100–107.
[3] Britton, C. et al., 2000, ''Multiple-Input Microcantilever Sensors,'' Ultramicroscopy, **82**(1–4), pp. 17–21.
[4] Moulin, A. et al., 2000, ''Microcantilever-Based Biosensors,'' Ultramicroscopy, **82**, pp. 23–31.
[5] Sarid, D., *Scanning Force Microscopy*, Oxford University Press, New York, 1994.
[6] Binning, G. et al., 1986, ''Atomic Force Microscope,'' Phys. Rev. Lett., **56**(9), pp. 930–933.
[7] Fritz, J. et al., 2000, ''Translating Biomolecular Recognition Into Nanomechanics,'' Science, **288**, pp. 316–318.
[8] Raiteri, R. et al., 1999, ''Sensing of Biological Substances Based on the Bending of Microfabricated Cantilevers,'' Sens. Actuators B, **61**, pp. 213–217.
[9] Chui, B. et al., 1998, ''Independent Detection of Vertical and Lateral Forces With a Sidewall-Implanted Dual-Axis Piezoresistive Cantilever,'' Appl. Phys. Lett., **72**(11), pp. 1388–1390.
[10] Tortonese, M., Barrett, R., and Quate, C., 1993, ''Atomic Resolution With an Atomic Force Microscope Using Piezoresistive Detection,'' Appl. Phys. Lett., **62**(8), pp. 834–836.
[11] Gaucher, P. et al., 1998, ''Piezoelectric Bimorph Cantilever for Actuation and Sensing Applications,'' J. Phys. IV, **8**, pp. 235–238.
[12] Itoh, T., Ohashi, T., and Suga, T., ''Piezoelectric Cantilever Array for Multiprobe Scanning Force Microscopy,'' in *Proc. of the IX Int. Workshop on MEMS, San Diego, CA*, pp. 451–455, 1996.
[13] Minne, S., Manalis, S., and Quate, C., 1995, ''Parallel Atomic Force Microscopy Using Cantilevers With Integrated Piezoresistive Sensors and Integrated Piezoelectric Actuators,'' Appl. Phys. Lett., **67**(26), pp. 3918–3920.
[14] Huang, Q., and Lee, N., 2000, ''A Simple Approach to Characterizing the Driving Force of Polysilicon Laterally Driven Thermal Microactuators,'' Sens. Actuators, A, **A80**(3), pp. 267–272.
[15] Attia, P. et al., 1998, ''Fabrication and Characterization of Electrostatically Driven Silicon Microbeams,'' Microelectron. J., **29**, pp. 641–44.
[16] Blanc, N. et al., 1996, ''Scanning Force Microscopy in the Dynamic Mode Using Microfabricated Capacitive Sensors,'' J. Vac. Sci. Technol. B, **14**(2), pp. 901–905.
[17] Shiba, Y. et al., 1998, ''Capacitive Afm Probe for High Speed Imaging,'' Trans. of the IEE of Japan, **118E**(12), pp. 647–50.
[18] Napoli, M., and Bamieh, B., ''Modeling and Observer Design for an Array of Electrostatically Actuated Microcantilevers,'' in *Proc. 40th IEEE Conf. on Dec. and Cont., Orlando FL*, December 2001.
[19] Salapaka, S. et al., 2002, ''High Bandwidth Nano-Positioner: A Robust Control Approach,'' Rev. Sci. Instrum., **73**(9), pp. 3232–41.
[20] Daniele, A. et al., ''Piezoelectric Scanners for Atomic Force Microscopes: Design of Lateral Sensors, Identification and Control,'' in *Proc. of the 1999 American Control Conference, San Diego, CA*, June 1999.
[21] Turner, K., ''Multi-Dimensional MEMS Motion Characterization Using Laser Vibrometry,'' in *Digest of Technical Papers Transducers'99, Sendai, Japan*, 1999.
[22] Arnold, V., *Mathematical Methods of Classical Mechanics*, Springer, 1988.
[23] McLachlan, N., *Theory and Applications of the Mathieu Functions*, Oxford University Press, London, 1951.
[24] Rand, R., *Lecture Notes on Nonlinear Vibrations*, available online http://www.tam.cornell.edu/randdocs/, 2001.
[25] Vidyasagar, M., *Nonlinear Systems Analysis*, SIAM, 1993.
[26] Zhang, W. et al., 2002, ''Effect of Cubic Nonlinearity on Auto-Parametrically Amplified Resonant MEMS Mass Sensor,'' Sens. Actuators, A, **A102**(1–2), pp. 139–150.
[27] Nagpal, K., and Khargonekar, P., 1991, ''Filtering and Smoothing in an H_∞ Setting,'' IEEE Trans. Autom. Control, **36**(2), pp. 152–66.
[28] Chen, T., and Francis, B., *Optimal Sampled-Data Control Systems*, Springer, 1995.
[29] Bamieh, B. et al., 1993, ''Minimization of the l^∞-Induced Norm for Sampled-Data Systems,'' IEEE Trans. on AC, **38**(5), pp. 717–32.